Comparative Biochemistry and Physiology, Part C 191 (2017) 109–116

Contents lists available at ScienceDirect

Comparative Biochemistry and Physiology, Part C

journal homepage: www.elsevier.com/locate/cbpc

Chronic MeHg exposure modifies the histone H3K4me3 epigenetic landscape in *Caenorhabditis elegans*

Martina Rudgalvyte [a,b], Juhani Peltonen [a], Merja Lakso [a], Garry Wong [b,*]

[a] A. I. Virtanen Institute for Molecular Sciences, Department of Neurobiology, University of Eastern Finland, Kuopio, Finland
[b] Faculty of Health Sciences, University of Macau, Macau, S.A.R., China

ARTICLE INFO

Article history:
Received 19 June 2016
Received in revised form 29 September 2016
Accepted 2 October 2016
Available online 04 October 2016

Keywords:
Chromatin immunoprecipitation sequencing (ChIP-seq)
RNA sequencing (RNA-seq)
Heavy metal
Epigenetics
Mercury

ABSTRACT

Methylmercury (MeHg) is a persistent environmental pollutant that occurs in the food chain, at occupational sites, and *via* medical procedures. Exposure in humans and animal models results in renal, neuro, and reproductive toxicities. In this study, we demonstrate that chronic exposure to MeHg (10 μM) causes epigenetic landscape modifications of histone H3K4 trimethylation (H3K4me3) marks in *Caenorhabditis elegans* using chromatin immuno-precipitation sequencing (ChIP-seq). The modifications correspond to the locations of 1467 genes with enhanced and 508 genes with reduced signals. Among enhanced genes are those encoding glutathione-S-transferases, lipocalin-related protein and a cuticular collagen. ChIP-seq enhancement of these genes was confirmed with increased mRNA expression levels revealed by qRT-PCR. Furthermore, we observed enhancement of H3K4me3 marks in these genes in animals exposed to MeHg *in utero* and assayed at L4 stage. *In utero* exposure enhanced marks without alterations in mRNA expression except for the *lpr-5* gene. Finally, knockdown of lipocalin-related protein gene *lpr-5*, which is involved in intercellular signaling, and cuticular collagen gene *dpy-7*, structural component of the cuticle, by RNA interference (RNAi) resulted in increased lethality of animals after MeHg exposure. Our results provide new data on the epigenetic landscape changes elicited by MeHg exposure, as well as describe a unique model for studying *in utero* effects of heavy metals. Together, these findings may help to understand the toxicological effects of MeHg at the molecular level.

1. Introduction

Methylmercury (MeHg) is an environmental pollutant and serious public health concern with exposure occurring through ingestion of contaminated fish and seafood, or *via* occupational and environmental routes (Clarkson, 1983). MeHg is a potent teratogen, retinotoxin, and neurotoxin that poses a risk during gestational, postnatal and adult developmental stages. Because of its strong affinity to SH- groups, MeHg binds the amino acid L-cysteine and is transported to tissues as a L-amino acid substrate (Yin et al., 2008). It crosses the blood-brain barrier and accumulates in brain, causing embryonic defects, developmental abnormalities, and neurological dysfunction while it can also cause muscle and joint pain, and gastrointestinal dysfunction. In higher doses, impairment or loss of vision may occur (Amin-Zaki et al., 1974; Kerper et al., 1992; Johansson et al., 2007). Exposure to MeHg also increases the production of reactive oxygen species and activates a complex cascade of stress related events including impairment of Ca^{2+} homeostasis, disruption of the electron transfer chain, and an increase in mitochondrial permeability (Vanduyn et al., 2010; Ceccatelli et al., 2010). Mitochondrial membrane potential collapse can then lead to an arrest of ATP synthesis and ultimately cell death. Although mitochondria are considered to be a primary target of MeHg, the ability to bind any cysteine-containing protein and to corrupt energy metabolism enables this toxicant to activate other stress response systems and involve other subcellular structures including the endoplasmic reticulum (ER), Golgi complex, lysosomes, and nuclear envelope (Vanduyn et al., 2010; Roos et al., 2012; Rudgalvyte et al., 2013).

The long-lasting effects of MeHg that occur after acute or *in utero* exposure suggests that epigenetic patterns in target cells and tissues may be altered. Heritable disturbances such as decreased cell proliferation, cellular senescence, cell cycle regulation, and abnormal mitochondrial function observed in MeHg non-treated daughter cells support the existence of an epigenetic effect. The same disturbances can be caused by genetic alterations, however there is lack of data demonstrating changes in the DNA sequence after MeHg exposure. Moreover, DNA methyltransferase is inhibited in MeHg treated cells (So et al., 2011) and decreased methylation levels due to MeHg exposure were shown to be passed to daughter cells (Bose et al., 2012). *In vivo* studies on wild animals feeding mostly on fish confirmed a hypomethylation effect on DNA (Pilsner et al., 2010). Several types of epigenetic modifications are known to exist including methylation of DNA, and methylation, acetylation, and phosphorylation of histone proteins (Suganuma and

* Corresponding author at: Faculty of Health Sciences, University of Macau, Taipa, Macau, S.A.R., China.
E-mail addresses: Garry.Wong@uef.fi, GarryGWong@umac.mo (G. Wong).

http://dx.doi.org/10.1016/j.cbpc.2016.10.001

Workman, 2008). These modifications are known to participate in crucial cell processes such as DNA replication, repair, and gene transcription. Histone modifications are more flexible than DNA methylation and these modifications can activate or suppress transcriptional activity. Histone modifications are also dependent upon the amino acid residue. For example, active regions are enriched in histone *H*3 trimethylation at lysine 4 while inactive regions contain a high number of histone *H*3 trimethylation at lysine 27 (Bernstein et al., 2005; Hawkins et al., 2010). Multiple heavy metals such as arsenic, lead, copper or cadmium, can change epigenetic patterns at both DNA and histone modification levels (Zhong and Mass, 2001; Barcia-Sanjurjo et al., 2013; Kang et al., 2004; Bihaqi et al., 2011). A mouse brain study revealed that after MeHg exposure, a reduced acetylation level of histone *H*3 and increased trimethylation of *H*3 at lysine 27 in the promoter region of brain-derived neurotrophic factor alters the gene expression profile due to epigenetic changes (Onishchenko et al., 2008).

We used the nematode *Caenorhabditis elegans* as a model to study epigenetic effects of MeHg due to its ease of handling and potential to uncover harmful effects in toxicological studies (Nass and Hamza, 2007). Notably, *C. elegans* and humans share similarities in parts of cellular signaling and stress response pathways. It was previously demonstrated that chronic MeHg exposure reduces brood size and numbers of viable eggs, causes delay in development, initiates stress response, and affects animal viability (Vanduyn et al., 2010). We also recently demonstrated the involvement of oxidative stress and endoplasmic reticulum stress markers in cellular response at the mRNA level after an acute MeHg exposure (Rudgalvyte et al., 2013).

In the present study, we identified modifications in trimethylation patterns of histone *H*3 on lysine 4 (H3K4me3), a marker of actively transcribed regions, in chromatin isolated from whole animals after chronic MeHg exposure. Mapping allowed us to identify genes in these regions and Gene ontology (GO) analysis allowed us to identify pathways altered. Comparing to data from our previous RNA-seq study (Rudgalvyte et al., 2013), we were able to determine if these methylation changes were correlated with transcriptional changes. We also analyzed histone H3K4me3 patterns on several genes in L4 stage animals previously exposed *in utero* to determine the persistence of these epigenetic changes. Our results show not only vast changes in epigenetic landscape, but also how individual genes are altered at the epigenetic level following exposure to a serious environmental toxicant.

2. Materials and methods

2.1. C. elegans maintenance

C. elegans wild-type (WT) Bristol N2 and RNAi-sensitive mutant NL2099 (*rrf-3(pk1426)*) strains used in this study were obtained from the Caenorhabditis Genetics Center (St. Paul, MA USA) and maintained at 20 °C on nematode growth media (NGM) plates containing OP-50 bacteria according to standard protocols (Brenner, 1974).

2.2. Synchronization, treatment and larvae development assay

Synchronization of the worms was carried out using potassium hypochlorite solution to bleach the gravid adults. Isolated embryos were washed 4× with M9 buffer and to obtain synchronized population incubated in M9 buffer with gentle rocking for 18 h at a room temperature. For chronic exposure in ChIP-seq, RNA-Seq and qRT-PCR experiments L1 larvae animals were placed on NGM plates ± MeHg (0, 10 μM) (CH_3HgCl, Sigma-Aldrich, St Louis, MO) and allowed to grow at 20 °C until reaching L4 stage just before adulthood. For acute MeHg treatment animals were grown until L4 stage and transferred onto an NGM plates containing MeHg (25 μM) for 4 hours. MeHg-containing plates were prepared adding MeHgCl solution to the NGM. Plates prepared fresh before use to avoid over drying and concentration change. For larval development assay L1 stage synchronized animals were placed on an NGM plates and incubated at 20 °C for 40 h. Plates were examined every 4 h and time of reaching L4 stage was scored. The experiment was repeated three times in triplicate using 50 worms for each replicate.

2.3. Chromatin immunoprecipitation (ChIP) from L4 larvae animals

For IP reaction control and MeHg-treated L4 larvae worms were collected, washed 4× with sterile water, centrifuged several times at 2000 rpm for 1 min to obtain tightly packed pellet and frozen immediately. Frozen material was ground using a cryo mortar, suspended in 1% formaldehyde in PBS solution to cross-link proteins to DNA and chromatin was sheared into a 150–800 base pair size range using a Branson ultrasonic dismembrator (Thermo Fisher Scientific, Waltham, USA). ChIP reactions were carried out according to Rechtsteiner et al. (2010) using ~20 μg of chromatin and 3 μl of H3K4me3 (Active Motif, Carlsbad, *CA*) antibody per reaction, leaving 10% of a starting material as input. Rabbit IgG antibody (Sigma, St. Louis, MO) or no antibody was used for a negative control. ChIP reaction was incubated with antibody at 4 °C overnight. Protein G-coupled Dynabeads (Thermo Fisher Scientific) were added and incubated for 2 h with rotation. Magnetic beads were extracted using DynaMag-2 magnet (Thermo Fisher Scientific) and washed at room temperature in FA buffer (50 mM HEPES, pH 7.5/ 1 mM EDTA, pH 8/1% TRITON X-100/ 0.1% sodium deoxycholate/ 150 mM NaCl) twice for 5 min, FA buffer with 500 mM NaCl once for 5 min, FA buffer with 1 M NaCl once settling beads right away, TEL buffer (0.25 M LiCl/ 1% NP-40/ 1% sodium deoxycholate/ 1 mM EDTA/ 10 mM Tris-HCl, pH 8.0) once for 5 min and TE buffer twice for 5 min. Eluted, RNase A/proteinase K treated and overnight reverse-crosslinked samples were cleaned using QIAquick PCR purification kit (Qiagen, Hilden, Germany). Antibody affinity was tested by qPCR method using *act-1* and *act-4* genes as a positive control and intergenic region sequences from chromosomes IV and X (primer sequences are shown in Table 1). The ChIP-seq experiments were performed in duplicate and DNAs immunoprecipitated were sequenced at the Millard and Muriel Jacobs Genetics and Genomics Laboratory of California Institute of Technology (Pasadena, *CA*. U.S.A.) on an Illumina HiSeq 2500 instrument. Sequences were obtained in single read 50 mode.

Table 1
Oligonucleotides used in the study.

Oligonucleotide sequences for ChIP verification were:	
act-1-5′-CACCTGATGAATTGTCCCAACTA;	*act-1-3′*-CTCGTCGTCACACATTTTGATT;
act-4-5′-GGGTTTAAAATTTCCAACAACCT;	*act-4-3′*-TATTTGCGAAACAATGCAAATC;
IV:109037005′-CCAACTGTTCGATTCT TGTTCA;	*IV:10903700-3′*-AGAAAGCTGGAATTCA AATGGA;
X:4958400-5′ TTGGGAAGTTTGAAGC ATATCA;	*X:4958400-3′*-TTGCAATCTAAAAATGGCA ATC;
gst-5-5′- GGTAAGAAGCTTGCTCAATC;	*gst-5-3′*- AATGCTGGAAGGAAGATGTC;
gst-38-5′- CATACAACCAGCTTCCAATG;	*gst-38-3′*- CTGGAAGATAGACGCTTGTG;
lpr-5-5′- TAAACCAACAGTGCCACCAG;	*lpr-5-3′*- CTGGAGCAGTGAAGAATGAC;
dpy-7-5′- GATCCAGAACCAGCATTCCC;	*dpy-7-3′*- AATGCCAGTTCCTCCAATCG;
atf-6-5′- GATGATCTCCTGCATAACCC;	*atf-6-3′*- TTTGCACAACTCAACGGTGG;
sir-2.1-5′- ACGATTCAGAAGTTGCGGTC;	*sir-2.1-3′*- GGAGTGGCACCATCATCAAG;
cnx-1-5′- TGGTGAACCGGAAATGGATG;	*cnx-1-3′*- GCTCCACTCTCCATTGTATT.
Oligonucleotide sequences for qRT-PCR reactions were:	
act-1-5′ TCGGTATGGGACAGAAGGAC;	*act-1-3′* CATCCCAGTTGGTGACGATA;
lpr-5-5′ ATGTATTTGCAAGAGATACT;	*lpr-5-3′* TCATTGACAACTGGTTCGTA;
dpy-7-5′-ATTGCCAGTGTGCTCATTCT;	*dpy-7-3′*-CTTCCATTGCTCTTCACCAA;
atf-6-5′- CGCCACAGAGACAATAAGAG;	*atf-6-3′*- TTCCGGTCTTCAGTAGATCC;
sir-2.1–5′-GTGTGTCGCGATTTCTGCTC;	*sir-2.1–3′*- CGATCCTCGTCAGATAGTAC;
gst-1-5′- CCAAAGATGATCTTCGGCCA;	*gst-1-3′*- TGAGCCCATTAAGACGAGCG;
gst-4-5′-CAGAGGAAGAAGCTTACGCT;	*gst-4-3′*-TCTTGGCCAGGAACTTATTG;
gst-5-5′-CCAGCATTGAAAGAAACCTG;	*gst-5-3′*- GAAATATGGACGAGCCTCAC;
gst-38-5′-GAGCCGGAGAGCTCTGCCCT;	*gst-38-3′*-CAAGATAACGAGCCATCGCG;
hsp-4-5′-GGATCAACCAGAATTCCAA AGG;	*hsp-4-3′*-TCAGGGTTGATTCCACGAGAT;
hsp-6-5′-GGACTTAAAGGTCGTTCCAT;	*hsp-6-3′*- GATCGTAGACAGCGATGATC.

2.4. ChIP-seq analysis

The number of reads obtained from MeHg non-treated duplicate samples were 34.7M/48.9M and 41.7M/29.3M from the IgG control and H3K4me3 samples, respectively. The number of reads, obtained from MeHg-treated samples were 31.0M/27.6M and 24.8M/27.5M from the IgG control and H3K4me3 samples, respectively. Reads were aligned to the *C. elegans* genome (WS220) using Bowtie 1.1.2 (Trapnell et al., 2009) allowing at most 2 mismatches and 10 alignments per read and reporting reads in the best stratum (–best and –strata). The percentage of mapped reads with at least one reported alignment ranged from 6–38% for all H_2O/MeHg treatment samples. The alignments were processed using MACS2 peak calling algorithm with false discovery rate-corrected *p*-values (q-values) of <0.01. A total of 2704 peaks were identified in IgG/H3K4me3 for MeHg-non-treated samples and 4098 peaks were identified in IgG/H3K4me3 for MeHg-treated samples. The nearest gene for the peaks was obtained using ChIPpeakAnno (Zhu et al., 2010). Gene enrichment analysis was performed using DAVID Functional Annotation Tool 6.7 (Huang et al., 2009).

2.5. RNA isolation and cDNA synthesis

Both control and MeHg-treated L4 stage worms were collected, washed 4× with sterile water and placed immediately into Trizol solution (Gibco-BRL, Gaithersberg, MD). Total RNA was isolated according to manufacturer's protocol using RiboPure RNA purification kit and quantitated on a Nanodrop device (Thermo Scientific, Wilmington, DE, USA). cDNA was synthetized using RevertAid RT reverse transcription kit (Thermo Scientific) according to manufacturer's protocol using 0.5 μg of total RNA as a template.

2.6. Quantitative real-time PCR (qRT-PCR)

Several genes were selected for verification using qRT-PCR method. Both worm ChIP and cDNA samples from isolated total RNAs were used for confirmation reactions. Gene specific oligonucleotide primers for qRT-PCR were designed using Primer-BLAST (Ye et al., 2012) and obtained from Oligomer OY (Helsinki, Finland). Maxima SYBR green qPCR Master mix (Thermo Fisher Scientific) was used for amplification reactions according to the manufacturer's protocol. Reactions were performed in iCycler 1.0 system (Biorad, Hercules, *CA*, USA). Three independent biological replicates in technical duplicates were used for this analysis. Quantitative differences were calculated using delta-deltaCT method (Livak and Schmittgen, 2001) normalized to *act-1* (gene expression) or input (ChIP reactions). Sequences for all primer sets used are listed in Table 1.

2.7. RNA interference and whole body vulnerability assay

RNA-mediated interference (RNAi) was performed as previously described (Rudgalvyte et al., 2016) using RNase III-deficient *Escherichia coli* bacteria strain HT115 (DE3) carrying L4440 vector with the gene fragments (*lpr-5* and *dpy-7*) (GeneService, Source BioScience, PLC, Nottingham, UK). Animals were exposed to MeHg (0, 10 or 20 μM) for 24 or 48 h. Worms were considered dead if a touch on the anterior end of the body with a wire pick did not cause any movement. Experiments were repeated at three different times in triplicate technical replicates each time, using 50 animals per replicate. Results are presented as an average ± SD.

2.8. Statistics

The results are presented as the average of 3 independent replicates ± S.D. For gene expression analysis fold changes were calculated using ΔΔCT method**.** The statistical analysis was performed using Student's *t*-test.

3. Results

3.1. ChIP-seq analysis of C. elegans chronically exposed to MeHg

In this study, 1975 genes with a modified H3K4me3 pattern were uncovered of which 1467 had an increased level of methylation and 508 had a reduced methylation level. The complete gene lists can be found in Supplementary Table 1. Among increased H3K4me3 genes we observed were cytochrome *c* encoding *cyc-2.1*, family members of the glutathione S-transferases (*gst-1*, *gst-5, gst-6, gst-10, gst-38*), mitochondria-specific chaperone *hsp-60*, unfolded protein response (UPR)-related cAMP-dependent transcription factor *atf-6* and lipocalin-related protein *lpr-5*. In the decreased methylation list, we uncovered another UPR sensor protein kinase *ire-1*, Ca^{2+}-binding ER membrane protein *cnx-1* and NAD-dependent protein deacetylase *sir-2.1*.

The data from ChIP-seq were compared to our previous RNA-Seq data where gene expression changes following MeHg treatment were investigated (Rudgalvyte et al., 2013). Overall, we found overlap of 43 genes up-regulated by RNA-Seq and increased methylation by ChIP-seq and 7 genes in down-regulated/decreased methylation lists (Table 2). We then compared mapped reads for selected genes that were on the overlapping lists: *gst-5, gst-38, lpr-5*, and *dpy-7* (Fig. 1). A large number of the 43 genes up regulated by RNA-seq and enhanced in H3K4me3 were from specific gene families that form or affect structures in the cuticle. These include dumpy (*dpy-3, dpy-7, dpy-9, dpy-8, dpy-5*), molting (*mlt-11, mlt-10, mlt-8*), collagen (*col-176, col.-110, col.-129*), blister (*bli-1, bli-2*), long (*lon-3*), and roller (*rol-6*) gene families (Table 2).

3.2. Functional annotation and GO enrichment analysis for H3K4me3 associated genes

In order to identify biological themes over-represented in our gene lists, DAVID functional annotation tool was used to annotate and extract gene groups that displayed significant ($p < 0.05$) enrichment of Gene Ontology (GO) biological processes, cellular compartments, or molecular functions (Fig. 2 and Supplementary Table 2). Enriched biological processes that were identified in lists for enriched H3K4me3 marks were: nematode larval development (209 genes), positive regulation of growth rate (181 genes), collagen and cuticulin-based cuticle development (19 genes), protein transport (30 genes), and translation (29 genes). A number of increased histone activity genes belong to the cellular component cytoplasm (134 genes), intracellular organelle (191 genes), nucleus (96 genes), mitochondrial part (14 genes) groups including ATP synthesis proteins ATP-synthase G homolog, ATP-synthase subunit, cytochrome *c*, and mitochondria-specific *hsp-60*. The most over-represented biological processes for reduced H3K4me3 were genitalia development (45 genes), positive regulation of growth rate (78 genes), meiosis (15 genes), and organ morphogenesis (21 genes). Enriched cellular component groups for decreased H3K4me3 were intracellular organelle (73), cytoplasm (43 genes), nucleus (43 genes), mitochondrial inner membrane (5 genes), and endoplasmic reticulum (8 genes). Interestingly, the GO category for positive regulation of growth rate was found on both enriched and reduced gene lists.

3.3. Confirmation of H3K4me3 methylation pattern changes by ChIP and qRT-PCR at selected gene regions in MeHg exposed animals

We selected a number of genes to verify the increased methylation level of H3K4me3 using ChIP and qRT-PCR methods. These included 2 glutathione S-transferases *gst-5* and *gst-38*, lipocalin-related protein *lpr-5*, cuticular collagen coding *dpy-7*, UPR-related cAMP-dependent transcription factor *atf-6*, and UPR sensor protein kinase *ire*-1. In addition to histone trimethylation pattern analysis, we performed gene expression analysis to determine if changes in methylation affected gene expression. Of all the genes tested, only *ire-1* showed no significant

Table 2
Forty three (43) up-regulated and 7 down-regulated genes in MeHg-treated compared to control *C. elegans* detected by RNA-Seq that correspond to ChIP-Seq enriched gene list using H3K3me3 antibody following MeHg exposure. FPKM values are fragments per kilobase of exon per million fragments mapped. Fold change values are from RNA-seq data.na, not available.

Transcript ID	WormBase locus ID (if available)	Fold change $FPKM_{MeHg}/FPKM_{control}$	FDR-corrected *p*-value (q-value)
Y64H9A.2	*na*	71.38	0.00
EGAP7.1	*dpy-3*	33.67	0.00
R07E3.6	*na*	32.82	0.00
W04G3.2	*lpr-5*	31.10	0.00
F46C8.6	*dpy-7*	21.24	0.00
W01F3.3	*mlt-11*	14.99	0.00
C09G5.6	*bli-1*	14.89	0.00
T21D12.2	*dpy-9*	14.78	3.70×10^{-11}
F52E4.6	*wrt-2*	14.48	1.71×10^{-9}
T14B4.6	*dpy-2*	13.03	1.13×10^{-9}
ZK1290.12	*wrt-1*	11.99	2.07×10^{-9}
C31H2.2	*dpy-8*	11.31	4.63×10^{-10}
C09E8.3	*mlt-10*	11.04	8.46×10^{-10}
Y39A1A.9	*na*	10.14	7.02×10^{-7}
Y55F3AM.14	*na*	7.78	3.07×10^{-5}
Y57E12B.3	*lipl-6*	6.99	2.75×10^{-3}
F59E12.12	*bli-2*	6.89	9.49×10^{-11}
Y46G5A.36	*na*	6.50	1.53×10^{-2}
ZK836.1	*lon-3*	6.27	3.18×10^{-7}
F47F6.1	*lin-42*	6.11	1.48×10^{-11}
T01B7.7	*rol-6*	6.09	4.23×10^{-8}
F29C12.1	*pqn-32*	5.87	5.09×10^{-12}
W08F4.6	*mlt-8*	5.70	6.48×10^{-10}
C02E7.7	*na*	5.18	1.24×10^{-6}
C42D8.5	*acn-1*	5.17	1.21×10^{-10}
F35E8.8	*gst-38*	4.94	9.58×10^{-7}
F27C1.8	*dpy-5*	4.23	0.00
ZC373.7	*col-176*	4.23	2.44×10^{-2}
Y58A7A.2	*na*	4.15	4.35×10^{-2}
F19C7.7	*col-110*	4.12	7.61×10^{-5}
F59B10.1	*pqn-47*	4.11	3.90×10^{-5}
Y80D3A.5	*cyp-42 A1*	3.92	8.93×10^{-3}
C29F9.2	*na*	3.76	2.90×10^{-2}
Y57A10A.23	*na*	3.72	1.90×10^{-5}
C50F2.6	*fkb-5*	3.28	1.11×10^{-4}
C05C8.3	*fkb-3*	3.01	3.84×10^{-3}
T19C3.2	*na*	2.96	2.94×10^{-3}
F15E6.2	*lgc-22*	2.71	1.37×10^{-2}
F48F7.2	*syx-2*	2.51	4.27×10^{-2}
R03D7.6	*gst-5*	2.32	4.41×10^{-2}
M88.6	*pan-1*	2.27	8.67×10^{-4}
ZC513.6	*oma-2*	2.09	3.10×10^{-2}
C17F4.7	*na*	2.05	3.20×10^{-2}
–	–	–	–
Y37E11B.9	*na*	0.08	3.53×10^{-2}
Y25C1 A.1	*clec-123*	0.35	1.04×10^{-2}
C50E10.1	*na*	0.38	2.85×10^{-2}
M18.1	*col-129*	0.40	3.88×10^{-3}
Y38C1 AA.7	*na*	0.41	5.86×10^{-3}
Y69A2AR.19	*na*	0.41	1.49×10^{-2}
T16H12.6	*kel-10*	0.42	4.38×10^{-2}

changes in both methylation and gene expression levels (data not shown). We observed significant increases in the rest of the selected H3K4me3 associated genes. Significant (≥2-fold change and $p < 0.05$) H3K4 trimethylation and gene expression changes were observed in *gst-5* (3.2-fold H3K4 trimethylation/8.2-fold gene expression), *gst-38* (2.7-fold/18.7-fold), *lpr-5* (3.2-fold/4.7-fold), *dpy-7* (3.5-fold/1.3-fold), and *atf*-6 (2.7-fold/1.1-fold) genes (Fig. 3a).

3.4. Persistence of H3K4me3 signal enrichment after in utero MeHg exposure

In order to determine if MeHg exposure induces effects in methylation pattern *in utero* that persists over a long-term period, we isolated embryos from gravid adults exposed to MeHg (10 μM) for 96 h. Embryos were allowed to grow until the L4 larval stage free of MeHg and analyzed. Although animals exposed *in utero* to MeHg did not superficially appear different from controls, development was slightly delayed (Fig. 3b). Moreover, using ChIP and qRT-PCR methods we observed increased H3K4me3 associated enhancement levels. For this experiment, we selected the same genes we used for confirmation: *gst-5, gst-38, lpr-5, dpy-7,* and *atf-6.* All of these genes demonstrated increased enhancement levels (≥2-fold change, $p < 0.05$). However, only *lpr-5* was found significantly up-regulated in gene expression (2.6-fold, $p < 0.05$) and other genes showed no significant increase (Fig. 3c).

3.5. Acute MeHg exposure increases GST and HSP gene expression in both naive and in utero pre-exposed animals

It has been shown that MeHg exposure induces ROS production in *C. elegans* and activates a cellular stress response (Vanduyn et al., 2010). We determined if early embryonic *in utero* MeHg exposure can modulate later stress responses to MeHg. We measured expression levels of several glutathione S-transferases (GSTs) and heat shock proteins (HSPs) that are known stress response genes after acute MeHg exposure (4 h, 25 μM) in naive or *in utero* pre-exposed animals. We observed a significant increase ($p < 0.05$) in *gst-4* (7.5-fold in naive/6.6-fold *in utero* pre-exposed), *gst-5* (6.6-fold/7.8-fold) and *gst-38* (7.2-fold/7.7-fold) gene expression. These results suggest that a previous *in utero* exposure to MeHg does not influence response to later acute MeHg exposure. No changes were observed in the expression of *gst-1* in any samples. No differences between samples were observed in *hsp-4* and *hsp-6* genes (Fig. 3d).

3.6. The lipocalin-related protein lpr-5 and cuticular collagen dpy-7 inhibits MeHg induced animal death

The lipocalin-related protein *lpr-5* and cuticular collagen *dpy-7* were selected from our gene lists to determine if these genes have an effect on animal vulnerability in presence of MeHg. RNAi experiments were performed to knock-down expressions of these genes. Since *lpr-5* knockdown animals suffer from body rupture during later reproductive stages, we decided to score death or survival after 24 h of exposure to eliminate additional effects of gene knock-down. *Dpy-7* animals were scored for death after 48 h of MeHg exposure. Our study revealed that RNAi of *lpr-5* and *dpy-7* resulted in increased vulnerability to death following MeHg exposure. After 24 h of MeHg exposure (20 μM), 25% of *lpr-5* knockdown animals were found dead, while WT animals tolerated the toxicant (Fig. 4a). The decrease of *dpy-7* expression resulted in a death of 63% (10 μM) and 97% (20 μM) of animals while only 3% (10 μM) and 5% (20 μM) of animals experienced death in WT control group (Fig. 4b). Results are presented as an average of three independent experiments ± S.D., $p < 0.05$. These results suggest that expression of *lpr-5* and *dpy-7* are essential in the inhibition of MeHg- induced animal death.

4. Discussion

We performed global chromatin immunoprecipitation sequencing (ChIP-Seq) to uncover H3K4me3 enriched and reduced regions after chronic MeHg exposure (10 μM) in the nematode *C. elegans.* Our results show enrichment in several glutathione S-transferases (*e.g. gst-1, gst-5, gst-6, gst-10* and *gst-38*), mitochondria-specific chaperone *hsp-60*, and unfolded protein response (UPR)-related cAMP-dependent transcription factor *atf-6.* Our results support previously reported UPR involvement in MeHg-induced toxicity (Rudgalvyte et al., 2013) and gene expression changes in GST family following MeHg exposure (Vanduyn et al., 2010; Rudgalvyte et al., 2013). Consistent with these results, a previous study has shown that prenatal exposure to MeHg can developmentally retard the glutathione system in mouse brain (Montgomery et al., 2008). Studies investigating the epigenetic regulation of the Gstz1 locus in developing mouse liver also show low levels of DNA

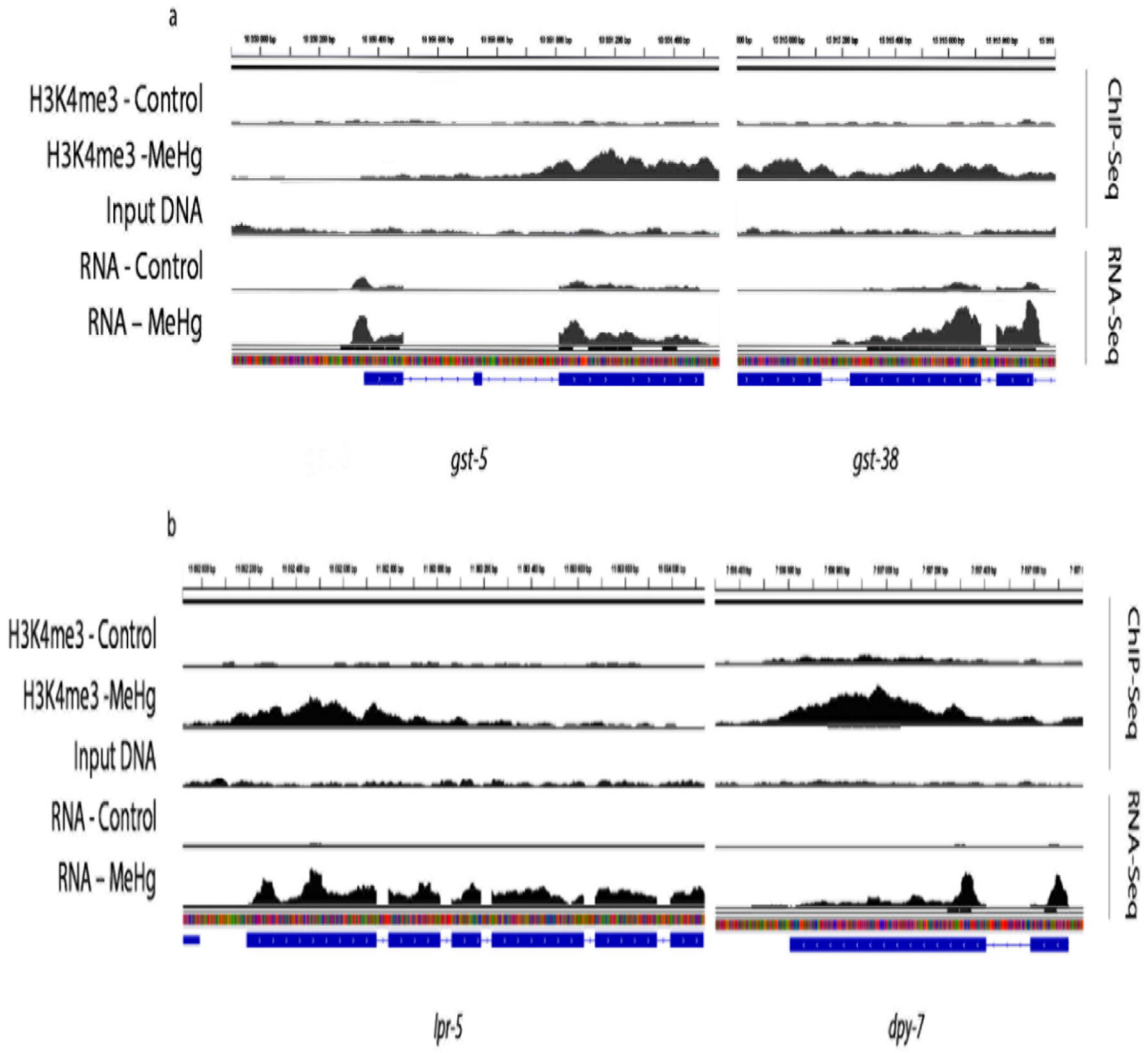

Fig. 1. ChIP-seq and RNA-seq in control treated and MeHg treated animals. (a) Chip-seq peaks were identified using H3K4Me3 antibody or input DNA as a control. MeHg treatment increased H3K4me3 signals in genes *gst-5, gst-38*. (b) Peaks from *lpr-5* and *dpy-7* genes. ChIP-Seq data (lines 1–3) and the corresponding genes were compared with RNA-Seq data (lines 4–5). Gene structure is shown at the bottom. Images were generated by Integrated Genome Viewer 2.3.

methylation and H3K27me3 gene reduction marks and enrichment of H3K4me2 gene activation marks (Cui et al., 2010). Our results showing both increases in mRNA expression levels and H3K4me3 marks in several GST genes suggests that our *C. elegans* model may correspond some elements of epigenetic regulation observed in higher organisms.

Although data in this study was obtained using the concentration of MeHg higher than normally can be encountered in the environment, previous studies using more environmentally relevant concentration for cell line treatment that correspond to Hg levels in the brain of fish consumers (Ceccatelli et al., 2013) and studying dental professionals (Goodrich et al., 2013) revealed epigenetic changes as the effect of MeHg toxicity, confirming that MeHg is an epigenetic toxicant. Using higher concentrations for animal treatment might help to uncover a wider range of pathways involved in MeHg-induced stress response and may also detect adverse effects sooner.

In addition, our study provides evidence for widespread epigenetic changes elicited by MeHg that can be correlated with changes in gene expression. We demonstrate that for some of the genes, these epigenetic changes persist. A previous study has shown that epigenetic changes are associated with long lasting adverse effects in stem cells induced by MeHg and these can be inherited (Bose et al., 2012). Other studies have shown epigenetic effects of mercury exposure in human tissues (Cardenas et al., 2015; Maccani et al., 2015). However, these studies looked at non target tissues such as umbilical cord blood (Cardenas et al., 2015) or placenta (Maccani et al., 2015) and direct epigenetic effects on the offspring remain unknown. In contrast to the human studies where offspring were not studied directly, mice studies (Pilones et al., 2009; Montgomery et al., 2008; Stringari et al., 2008) looked at tissues or behaviors in individual adult animals exposed to mercury *in utero* during the sensitive gestation period, however, epigenetic analyses were not performed. Our studies with *C. elegans* were aimed to bridge these two approaches where we were able to expose animals *in utero*, demonstrate a developmental phenotype, and provide evidence of epigenetic changes in specific genes directly in the affected animal after the *in utero* exposure. The results of long lasting increase in H3K4me3 signals but non-correlation with RNA expression levels after *in utero* exposure suggests complex gene regulatory mechanisms. Other histone modifications or epigenetic changes (methylated DNA, miRNA, *etc.*) may ultimately compensate for long lasting marks. Many more epigenetic marks that are associated with increased or decreased transcription will need to be explored in future studies to discern the changes that ultimately result in RNA expression. We also observed that while H3K4me3 marks remain after *in utero* exposure, they do not confer an additive effect.

We observed upregulation and epigenetic activation of gene *lpr-5* that belongs to the calycin sub-family of lipocalin-related proteins expressed in *C. elegans* in all stages from embryos to adults. RNAi

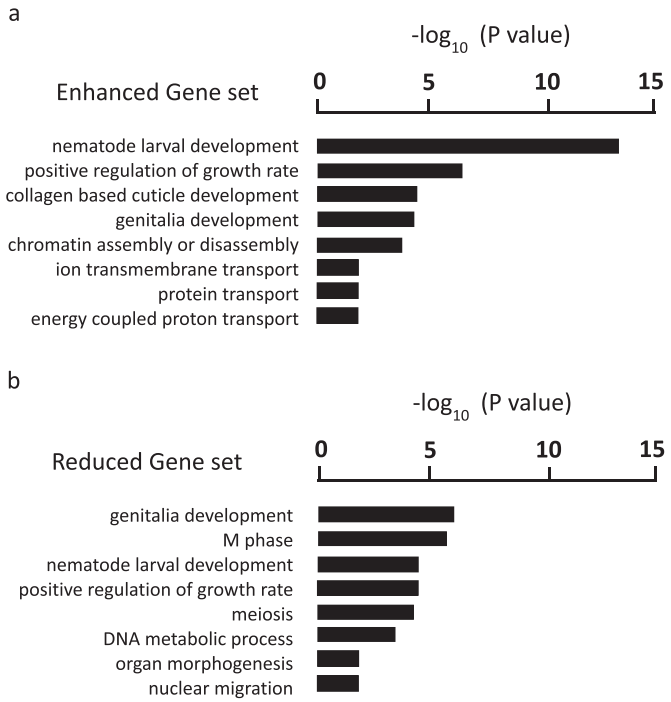

Fig. 2. Gene ontology (GO) categories significantly enriched in gene lists of MeHg treated animals. (a) Chip-seq H3K4me3 list of enhanced genes (1467 total) was analyzed for GO category (biological process, molecular function, cellular compartment) enrichment using DAVID annotation tool as described in Methods. Bar indicates level of significance. (b) GO category enrichment from Chip-seq lists of genes reduced (508 total) after MeHg treatment.

knockdown of this gene resulted in decreased animal survival after MeHg exposure. Moreover, reduced *lpr-5* activity caused an egg laying defective phenotype in control animals causing body rupture. An *lpr-5* promoter-GFP reporter transgene indicates that this gene is expressed in seam cells of the hypodermis (Thoemke et al., 2005). Our data suggests *lpr-5* involvement in the development of intact epithelium and knock down of this gene may result in lost protection from environmental toxicants. In support of this we previously found that *lpr-5* RNAi also made animals more sensitive to $MnCl_2$ toxicity (Rudgalvyte et al., 2016). In humans, neutrophil gelatinase-associated lipocalin (NGAL) has been proposed as a biomarker for renal injury that may occur during transplants, bypass surgeries, or xenobiotic toxicity including mercury (Mishra et al., 2005). Another lipocalin-related protein *lpr-1* was found to be involved in excretory system development in *C. elegans* (Stone et al., 2009) and suggests another structure that may be affected by MeHg. Whether the excretory system of *C. elegans* mimics the renal system of humans remains to be seen, yet it appears that the lipocalin related (LPR) proteins are affected in both systems. Further work on defining the function of LPR family genes is necessary to determine how closely excretory systems are between humans and *C. elegans*.

In addition, inactivation of cuticular collagen *dpy-7* resulted in increased animal lethality after MeHg exposure. Another study has shown increased sensitivity to bisphenol A of *dpy-7* mutant animals (Watanabe et al., 2005) further suggesting that intact epithelium may play an important role in animal protection against environmental toxicants. DPY-7 is highly conserved across species and homologous to human Isoform 2 of Collagen alpha-1(XVII) chain. These results would predict that *dyp-7* mutants would be sensitive to a large range of toxins. Coupled with results from *lpr-5*, the loss of epithelial integrity may allow easier absorption of toxicants and could explain the increased sensitivity of *lpr-5* and *dpy-7* to MeHg in *C. elegans*. In support of this,

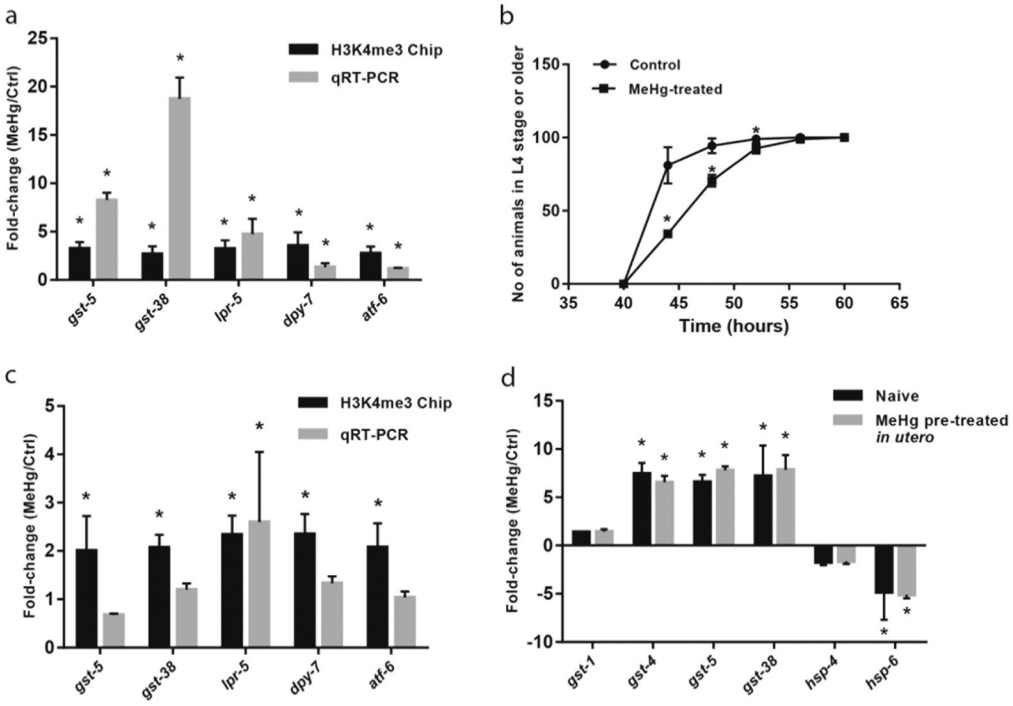

Fig. 3. ChIP and qRT-PCR analysis of specific genes. (a) H3K4me3 ChIP and qRT-PCR were performed on selected genes to confirm Chip-seq and RNA-seq results after chronic MeHg treatment (10 μM) in L4 stage animals. Filled black bars represent H3K4me3 ChIP values and filled grey bars represent gene expression changes in MeHg exposed animals. qRT-PCR results are presented as the average from 3 independent samples ± S.D. Fold changes were calculated using ΔΔCT method. (b) Development of animals exposed to MeHg *in utero*. Animals were allowed to hatch and the time to reach L4 stage was observed by following development every 4 h. Observations were started 40 h after placing L1 stage worms on NGM. Assays were performed three times with three replicates each time and 50 animals per replicate. Results are presented as average ± SD. (c) H3K4me3 ChIP and qRT-PCR analysis on animals exposed to MeHg *in utero* and analyzed at L4 stage. (d) qRT-PCR analysis on GST and HSP family genes after acute MeHg exposure (4 h, 25 μM) in naive or *in utero* MeHg pre-treated animals. Filled black bars represent gene expression of L4 stage naive animals treated with MeHg for the first time. Filled grey bars represent gene expression in L4 stage animals treated with MeHg after pre-treatment with MeHg *in utero*. Negative fold changes were calculated based on −1 treated/control. *, Significant difference from control with >2-fold change and $p < 0.05$. Figures were created using GraphPad Prism software.

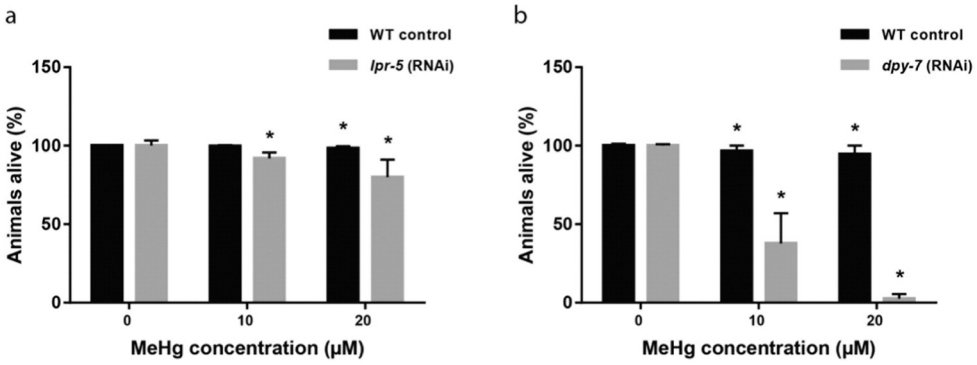

Fig. 4. Role of *lpr-5* and *dpy-7* gene in mediating MeHg induced lethality. (a) The RNAi-sensitive strain NL2099 (*rrf-3*) was grown for 48 h on plates with the *lpr-5* RNAi bacteria clone or empty vector (WT control) containing bacteria at L4 stage and transferred onto MeHg (10 μM or 20 μM as indicated) plates for 24 h (*lpr-5*). (b) RNAi assay for 48 h with *dpy-7* bacteria. The number of dead worms was then scored. The experiment was repeated three times in triplicates counting at least 50 animals per replicate. Results are presented as average ± SD. *, RNAi (*lpr-5* or *dpy-7*) is significantly different from WT control, *t*-test, $p < 0.05$. Figures were created using GraphPad Prism software.

we observed that a large proportion of cuticle proteins were both enhanced in H3K4me3 marks and upregulated in gene expression. These included a family of dumpy (*dyp*), molting (*mlt*), blister (*bli*), long (*lon*), roller (*rol*) and collagen (*col*) genes (Table 2). This was also seen in the enriched GO biological process groups (Fig. 2, Supplementary Table 2). As MeHg may bind to cysteine residues on the cuticle surface, cuticular genes may provide the first response to environmental toxicants in our exposure system. Loss of epithelial integrity is a fairly severe response to high level MeHg toxicity that might not be a major concern for vertebrates effected by lower environmental concentrations. Yet, in more severe poisoning cases, dermal toxicity or epithelium exposure may be an important and overlooked aspect of MeHg's harmful effects.

5. Conclusion

To our knowledge, this is the first global histone 3 at lysine 4 trimethylation pattern analysis following acute MeHg exposure. Our study presents new insights into molecular effects of MeHg at the epigenetic level that are manifested at transcriptional levels. Moreover, our results support the notion that MeHg causes long-lasting effects *via in utero* exposure and suggests a novel model for studying transgenerational effects of heavy metals. Our investigation also provides a new source of data for further studies for molecular toxicologists to investigate specific genes that are affected following methyl mercury exposure. Finally, we highlight effects on genes important for cuticle formation and structure that are sensitive to MeHg exposure.

Supplementary data to this article can be found online at http://dx.doi.org/10.1016/j.cbpc.2016.10.001.

Conflict of interests

The authors declare that they have no conflicts of interest.

Acknowledgements

We thank Drs. Igor Antoshechkin for sequencing and Carina Holmberg-Still for providing the *lpr-5* RNAi clone. Yvonne Lussi, Luca Mariani, Marjo Malinen, Yang Yang, and Liisa Salcini are gratefully acknowledged for their advice and protocols. Some strains were provided by the CGC, which is funded by NIH Office of Research Infrastructure Programs (P40 OD010440). This study was supported in part by the Academy of Finland Project 62340 and grant MYRG2015-00231-FHS from the University of Macau.

References

Amin-Zaki, L., Elhassani, S., Majeed, M.A., Clarkson, T.W., Doherty, R.A., Greenwood, M.R., 1974. Studies of infants postnatally exposed to methylmercury. J. Pediatr. 85 (1), 81–84.
Barcia-Sanjurjo, I., Vazquez-Cedeira, M., Barcia, R., Lazo, P.A., 2013. Sensitivity of the kinase activity of human vaccinia-related kinase proteins to toxic metals. J. Biol. Inorg. Chem. 18 (4), 473–482.
Bernstein, B.E., Kamal, M., Lindblad-Toh, K., Bekiranov, S., Bailey, D.K., Huebert, D.J., McMahon, S., Karlsson, E.K., Kulbokas III, E.J., Gingeras, T.R., Schreiber, S.L., Lander, E.S., 2005. Genomic maps and comparative analysis of histone modifications in human and mouse. Cell 120 (2), 169–181.
Bihaqi, S.W., Huang, H., Wu, J., Zawia, N.H., 2011. Infant exposure to lead (Pb) and epigenetic modifications in the aging primate brain: implications for Alzheimer's disease. J. Alzheimers Dis. 27 (4), 819–833.
Bose, R., Onishchenko, N., Edoff, K., Janson Lang, A.M., Ceccatelli, S., 2012. Inherited effects of low-dose exposure to methylmercury in neural stem cells. Toxicol. Sci. 130 (2), 383–390.
Brenner, S., 1974. The genetics of *Caenorhabditis elegans*. Genetics 77, 71–94.
Cardenas, A., Koestler, D.C., Houseman, E.A., Jackson, B.P., Kile, M.L., Karagas, M.R., et al., 2015. Differential DNA methylation in umbilical cord blood of infants exposed to mercury and arsenic in utero. Epigenetics 10 (6), 508–515.
Ceccatelli, S., Dare, E., Moors, M., 2010. Methylmercury-induced neurotoxicity and apoptosis. Chem. Biol. Interact. 188 (2), 301–308.
Ceccatelli, S., Bose, R., Edoff, K., Onishchenko, N., Spulber, S., 2013. Long-lasting effects of exposure to methylmercury during development. J. Intern. Med. 273 (5), 490–497.
Clarkson, T.W., 1983. Mercury. Annu. Rev. Public Health 4, 375–380.
Cui, J.Y., Choudhuri, S., Knight, T.R., Klaassen, C.D., 2010. Genetic and epigenetic regulation and expression signatures of glutathione S-transferases in developing mouse liver. Toxicol. Sci. 116 (1), 32–43.
Goodrich, J.M., Basu, N., Franzblau, A., Dolinoy, D.C., 2013. Mercury biomarkers and the DNA methylation among Michigan dental professionals. Environ. Mol. Mutagen. 54 (3), 195–203.
Hawkins, R.D., Hon, G.C., Lee, L.K., Ngo, Q., Lister, R., Pelizzola, M., Edsall, L.E., Kuan, S., Luu, Y., Klugman, S., et al., 2010. Distinct epigenomic landscapes of pluripotent and lineage-committed human cells. Cell Stem Cell 6 (5), 479–491.
Huang, D.W., Sherman, B.T., Lempicki, R.A., 2009. Systematic and integrative analysis of large gene lists using DAVID Bioinformatics Resources. Nat. Protoc. 4, 44–57.
Johansson, C., Castoldi, A.F., Onishchenko, N., Manzo, L., Vahter, M., Ceccatelli, S., 2007. Neurobehavioral and molecular changes induced by methylmercury exposure during development. Neurotox. Res. 11 (3–4), 241–260.
Kang, J., Lin, C., Chen, J., Liu, Q., 2004. Copper induces histone hypoacetylation through directly inhibiting histone acetyltransferase activity. Chem. Biol. Interact. 148 (3), 115–123.
Kerper, L.E., Ballatori, N., Clarkson, T.W., 1992. Methylmercury transport across the blood-brain barrier by an amino acid carrier. Am. J. Phys. 262 (5 Pt 2), R761–R765.
Livak, K., Schmittgen, T.D., 2001. Analysis of relative gene expression data using real-time quantitative PCR and the 2-ΔΔCt method. Methods 25, 402–408.
Maccani, J.Z., Koestler, D.C., Lester, B., Houseman, E.A., Armstrong, D.A., Kelsey, K.T., et al., 2015. Placental DNA methylation related to both infant toenail mercury and adverse neurobehavioral outcomes. Environ. Health Perspect. 123 (7), 723–729.
Mishra, J., Dent, C., Tarabishi, R., Mitsnefes, M.M., Ma, Q., Kelly, C., et al., 2005. Neutrophil gelatinase-associated lipocalin (NGAL) as a biomarker for acute renal injury after cardiac surgery. Lancet 365 (9466), 1231–1238.
Montgomery, K.S., Mackey, J., Thuett, K., Ginestra, S., Bizon, J.L., Abbott, L.C., 2008. Chronic, low-dose prenatal exposure to methylmercury impairs motor and mnemonic function in adult C57/B6 mice. Behav. Brain Res. 191 (1), 55–61.
Nass, R., Hamza, I., 2007. The nematode *C. elegans* as an animal model to explore toxicology in vivo: solid and axenic growth culture conditions and compound exposure parameters. Curr. Protoc. Toxicol. (Chapter 1, Unit1.9).
Onishchenko, N., Karpova, N., Sabri, F., Castren, E., Ceccatelli, S., 2008. Long-lasting depression-like behavior and epigenetic changes of BDNF gene expression induced by perinatal exposure to methylmercury. J. Neurochem. 106 (3), 1378–1387.

Pilones, K., Tatum, A., Gavalchin, J., 2009. Gestational exposure to mercury leads to persistent changes in T-cell phenotype and function in adult DBF1 mice. J. Immunotoxicol. 6 (3), 161–170.

Pilsner, J.R., Lazarus, A.L., Nam, D.H., Letcher, R.J., Sonne, C., Dietz, R., et al., 2010. Mercury-associated DNA hypomethylation in polar bear brains via the LUminometric methylation assay: a sensitive method to study epigenetics in wildlife. Mol. Ecol. 19 (2), 307–314.

Rechtsteiner, A., Ercan, S., Takasaki, T., Phippen, T.M., Egelhofer, T.A., Wang, W., Kimura, H., Lieb, J.D., Strome, S., 2010. The histone H3K36 methyltransferase MES-4 acts epigenetically to transmit the memory of germline gene expression to progeny. PLoS Genet. 6 (9), e1001091.

Roos, D., Seeger, R., Puntel, R., Barbosa, N.V., 2012. Role of calcium and mitochondria in MeHg-mediated cytotoxicity. J. Biomed. Biotechnol. 2012, 248764.

Rudgalvyte, M., VanDuyn, N., Aarnio, V., Heikkinen, L., Peltonen, J., Lakso, M., Nass, R., Wong, G., 2013. Methylmercury exposure increases lipocalin related (lpr) and decreases activated in blocked unfolded protein response (abu) genes and specific miRNAs in *Caenorhabditis elegans*. Toxicol. Lett. 222, 189–196.

Rudgalvyte, M., Peltonen, J., Lakso, M., Nass, R., Wong, G., 2016. RNA-seq reveals acute manganese exposure increases endoplasmic reticulum related and lipocalin mRNAs in *Caenorhabditis elegans*. J. Biochem. Mol. Toxicol. 30 (2), 97–105.

So, A.Y., Jung, J.W., Lee, S., Kim, H.S., Kang, K.S., 2011. DNA methyltransferase controls stem cell aging by regulating BMI1 and EZH2 through microRNAs. PLoS One 6 (5), e19503.

Stone, C.E., Hall, D.H., Sundaram, M.V., 2009. Lipocalin signaling controls unicellular tube development in the *Caenorhabditis elegans* excretory system. Dev. Biol. 329 (2), 201–211.

Stringari, J., Nunes, A.K., Franco, J.L., Bohrer, D., Garcia, S.C., Dafre, A.L., et al., 2008. Prenatal methylmercury exposure hampers glutathione antioxidant system ontogenesis and causes long-lasting oxidative stress in the mouse brain. Toxicol. Appl. Pharmacol. 227 (1), 147–154.

Suganuma, T., Workman, J.L., 2008. Crosstalk among histone modifications. Cell 135 (4), 604–607.

Thoemke, K., Yi, W., Ross, J.M., Kim, S., Reinke, V., Zarkower, D., 2005. Genome-wide analysis of sex-enriched gene expression during *C. elegans* larval development. Dev. Biol. 284 (2), 500–508.

Trapnell, C., Pachter, L., Salzberg, S.L., 2009. TopHat: discovering splice junctions with RNA-seq. Bioinformatics 25, 1105–1111.

Vanduyn, N., Settivari, R., Wong, G., Nass, R., 2010. SKN-1/Nrf2 inhibits dopamine neuron degeneration in a *Caenorhabditis elegans* model of methylmercury toxicity. Toxicol. Sci. 118 (2), 613–624.

Watanabe, M., Mitani, N., Ishii, N., Miki, K., 2005. A mutation in a cuticle collagen causes hypersensitivity to the endocrine disrupting chemical, bisphenol A, in *Caenorhabditis elegans*. Mutat. Res. 570 (1), 71–80.

Ye, J., Coulouris, G., Zaretskaya, I., Cutcutache, I., Rozen, S., Madden, T.L., 2012. Primer-BLAST: a tool to design target-specific primers for polymerase chain reaction. BMC Bioinf. 13, 134.

Yin, Z., Jiang, H., Syversen, T., Rocha, J.B., Farina, M., Aschner, M., 2008. The methylmercury-L-cysteine conjugate is a substrate for the L-type large neutral amino acid transporter. J. Neurochem. 107 (4), 1083–1090.

Zhong, C.X., Mass, M.J., 2001. Both hypomethylation and hypermethylation of DNA associated with arsenite exposure in cultures of human cells identified by methylation-sensitive arbitrarily-primed PCR. Toxicol. Lett. 122 (3), 223–234.

Zhu, L.J., Gazin, C., Lawson, N.D., Pages, H., Lin, S.M., Lapointe, D.S., Green, M.R., 2010. ChIPpeakAnno: a bioconductor package to annotate ChIP-seq and ChIP-chip data. BMC Bioinf. 11, 237.